Progress In Electromagnetics Research B, Vol. 55, 297–324, 2013

LOCALIZATION OF 3D NEAR-FIELD SOURCE USING THE APERTURE EXTENSION METHOD AND NONUNIFORM CROSS ARRAY

Jiajia Jiang*, Fajie Duan, Yanchao Li, and Xiangning Hua

The State Key Lab of Precision Measuring Technology & Instruments, Tianjin University, Tianjin, China

Abstract—Depending on the aperture extension (AE), a high performance three-dimensional (3D) near-field (NF) source localization algorithm is proposed with the nonuniform linear array (NLA). The proposed algorithm first generates some fictitious sensors to extend the array aperture by constructing a new Toeplitz matrix, and then obtains a two-dimensional (2D) covariance matrix which only contains the elevation angle and range parameters, and another 3D covariance matrix which contains the elevation/azimuth angle and range parameters. Then based on the 2D covariance matrix, both the elevation angle and range parameters are estimated by using the NLA along the Z axis. With the estimates of both the elevation angle and range parameters and combining the 3D covariance matrix, the estimates of the azimuth angle parameters are obtained using the NLA along the Y axis. The proposed algorithm has four main merits: i) unlike some classical NF source localization algorithms, the quarter-wavelength sensor spacing constraint is not required and more sources can be located simultaneously by the proposed algorithm; ii) the 3D parameters of the proposed algorithm are paired automatically; iii) the 3D search required in conventional 3D multiple signal classification (MUSIC) algorithm is replaced with only one-dimensional (1D) search, and thus the computational burden is reduced; iv) the proposed algorithm gains superior parameter estimation accuracy and resolution.

Received 13 July 2013, Accepted 14 October 2013, Scheduled 18 October 2013

* Corresponding author: Jia-Jia Jiang (tmjiangjiajia@163.com).

1. INTRODUCTION

Passive source localization using an array of sensors is an important topic in various signal processing fields, including radar, sonar, speech, communications, etc. [1]. For the 1D and 2D angles estimation of the far-field (FF) sources, many algorithms [2–11] have been proposed. However, when a source is in the *Fresnel* region of the array aperture [2–5], those algorithms in [2–11] will fail to locate sources. Therefore, for the NF source localization issue, some other algorithms [12–25] are also developed. More specifically, for 2D NF sources localization, Swindlehurst and Kailath proposed a spatial Wigner distribution approach [12], however, this method has a less-than-ideal estimation accuracy. Later on, Huang and Barkat [13] developed a 2D MUSIC method with high resolution, but it requires 2D search and thus has huge amount of computations. In addition, some other algorithms, such as the higher order ESPRIT-Like algorithm [14], the subspace-based (SB) algorithm [15], the two steps (TS) algorithm [16], and the weighted linear prediction (WLP) algorithm [17] are also presented to locate the NF source.

However, in many practical applications, different sources are located at different planes, and thus the 2D NF localization methods are no longer applicable [18–25] for 3D NF sources. Accordingly, some valuable algorithms [18–25] have been proposed for 3D NF sources localization. In [18, 19], based on cumulant matrices, a 3D NF source localization algorithm with a centro-symmetric cross array in the X-Y plane was presented, while it has a large amount of computation, is applicable only for non-Gaussian sources and requires a parameters pair-matching procedure. With a centro-symmetric cross array in the X-Y plane, R. N. Challa et al. presented a second-order-statistics (SOS) based solution [20] to locate the 3D NF sources, while it also requires a parameters pair-matching procedure. In [21, 22], at first, a 3D MUSIC localization algorithm is proposed and then improved so as to decrease the computational cost. Lee et al. [23] proposed an efficient localization algorithm for three uniform linear arrays (ULAs) in a Y-shape, whereby source locations are estimated by solving three nonlinear algebraic equations using three 1D incident angles obtained from subarrays under the FF assumption. In [24], with a uniform circular array (UCA), a path-following algorithm for localizing 3D NF source was proposed. In [25], based on the expectation and maximization method, a maximum likelihood 3D NF source localization algorithm was developed which requires a huge amount of computations.

The above-mentioned 2D [14–17] and 3D [18–25] NF source

localization algorithms have one or more main constraints: i) the number of source that they can deal with at most is not more than the half of number of array sensors; ii) the inter-sensor spacing of the array is within the quarter-wavelength of sources; iii) the extra parameters pair-matching procedure is required; iv) the computational cost is large.

To overcome the shortages of the conventional NF source localization algorithms [14–25], this paper develops a novel AE-based NF localization algorithm to jointly estimate the elevation/azimuth angle and range parameters of the 3D NF sources. Firstly, the proposed algorithm inserts some "zero" elements into the output vector $\bar{\mathbf{z}}(t)$ of the NLA along Z axis so as to constructs a new array output vector $\bar{\mathbf{z}}'(t)$ which is corresponding to a ULA. Considering that the covariance matrix $\bar{\mathbf{R}}_z = E\{\bar{\mathbf{z}}'(t)\bar{\mathbf{z}}'^H(t)\}$ is not a Hermitain Toeplitz matrix, by replacing each element with the average value of all elements on the same each diagonal line which is paralleled to the main diagonal line, a new Hermitain Toeplitz matrix $\bar{\mathbf{R}}_{zT}$ is constructed from $\bar{\mathbf{R}}_z$, and this Hermitain Toeplitz matrix is proved to be equal to the covariance matrix $\mathbf{R}_z$ which is generated by a ULA. Secondly, based on the constructed matrix $\bar{\mathbf{R}}_{zT}$, the elevation angle parameters are extracted and then are estimated by means of 1D search, and with the estimated elevation angle parameters, a free-search method is introduced to obtain the range parameter estimates of sources. Thirdly, similar to the constructed process of the Hermitain Toeplitz matrix $\bar{\mathbf{R}}_{zT}$, based on the NLA along Y axis a Hermitain Toeplitz matrix $\bar{\mathbf{R}}_{yT}$ is also constructed and proved to be equal to the covariance matrix $\mathbf{R}_y$ which is generated by a ULA. Finally, with the elevation angle and range estimates, the estimation process of the azimuth angle parameters is achieved using the matrix $\bar{\mathbf{R}}_{yT}$. The main contributions of this paper include: i) a special sparse array is introduced to extend the array aperture so as to improve resolution ability through the construction of the new Toeplitz matrix, ii) only SOS rather than higher-order statistics (HOS), and 1D search are used to estimate the elevation/azimuth angles parameters (Note that the range parameters estimation does not require any search procedure), iii) the 3D parameters can be paired automatically. Compared with the conventional methods, the proposed algorithm has moderate computation complexity, and provides superior resolution ability and improved parameter estimation accuracy.

The following notations will be used throughout. Superscripts T, H and $*$ represent the transpose, conjugate transpose and complex conjugate respectively, while $\arg(\cdot)$ is used to calculate phase.

2. DATA MODEL

2.1. Review of Data Model of the Uniform Linear Array

Consider K narrowband, independent radiating NF sources impinge on a ULA with $4M-1$ sensors (Fig. 1). Let the array center be the phase reference point as [14–20].

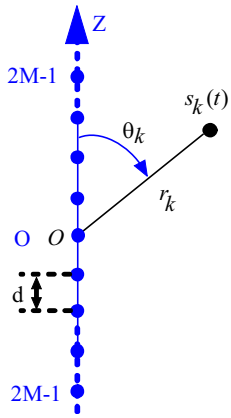

Figure 1. The array configuration.

The baseband signal representation of the t-th snapshot of the ULA output measured is expressed as

$$\mathbf{z}(t) = \sum_{k=1}^{K} \mathbf{a}_z(\theta_k, r_k) s_k(t) + n_z(t) = \mathbf{A}_z \mathbf{s}(t) + \mathbf{n}_z(t) \tag{1}$$

where $\mathbf{z}(t) = [z_{-2M+1}(t), \ldots, z_0(t), \ldots, z_{2M-1}(t)]^T$ is a $(4M-1)\times 1$ complex vector of observations at time t from $4M-1$ sensors, $\mathbf{s}(t) = [s_1(t), \ldots, s_K(t)]^T$ is a $K \times 1$ NF sources vector, $\mathbf{n}_z(t) = [n_{z,-2M+1}(t), \ldots, n_{z,0}(t), \ldots, n_{z,2M-1}(t)]^T$ is a array noise vector, and $\mathbf{a}_z(\theta_k, r_k)$ is the steering vector [14–20] represented by $\mathbf{a}_z(\theta_k, r_k) = [a_{z,-2M+1}(\theta_k, r_k), \ldots, a_{z,0}(\theta_k, r_k), \ldots, a_{z,2M-1}(\theta_k, r_k)]^T$ with

$$\begin{aligned}\mathbf{a}_z(\theta_k, r_k) &= \mathbf{a}_z(\varsigma_{z,k}, \xi_{z,k}) \\ &= \Big[e^{j[(-2M+1)\varsigma_{z,k}+(-2M+1)^2\xi_{z,k}]}, e^{j[(-2M+2)\varsigma_{z,k}+(-2M+2)^2\xi_{z,k}]}, \\ &\quad e^{j[(-2M+3)\varsigma_{z,k}+(-2M+3)^2\xi_{z,k}]}, \ldots, e^{j[m\varsigma_{z,k}+m^2\xi_{z,k}]}, \ldots, \\ &\quad e^{j[(2M-2)\varsigma_{z,k}+(2M-2)^2\xi_{z,k}]}, e^{j[(2M-1)\varsigma_{z,k}+(2M-1)^2\xi_{z,k}]}\Big]^T\end{aligned} \tag{2}$$

where

$$\varsigma_{z,k} = -\frac{2\pi d}{\lambda}\cos\theta_k \tag{3}$$

$$\xi_{z,k} = \frac{\pi d^2}{\lambda r_k}\sin^2\theta_k \tag{4}$$

λ is the signal carrier wavelength, $\theta_k \in [0, \pi]$ and $r_k \in (0.62(D^3/\lambda)^{1/2}, 2D^2/\lambda)$ [14–17] with D representing the array aperture denote the elevation angle and range of the k-th source, respectively, and d is the inter-sensor spacing between the ULA sensors. $\mathbf{A}_z$ is the array manifold matrix formed by the steering vectors and is given by

$$\mathbf{A}_z = [\mathbf{a}_z(\varsigma_{z,1}, \xi_{z,1}), \mathbf{a}_z(\varsigma_{z,2}, \xi_{z,2}), \ldots, \mathbf{a}_z(\varsigma_{z,K}, \xi_{z,K})] \tag{5}$$

Based on the definition of the array output covariance matrix [2–25], it is well known that the array output covariance matrix $\mathbf{R}_z$ of the ULA is a Hermitain Toeplitz matrix, and can be expressed as

$$\mathbf{R}_z = (r_{z,ij}) = E\{\mathbf{z}(t)\mathbf{z}^H(t)\} = \begin{bmatrix} \rho_{z,1} & \rho_{z,2}^* & \rho_{z,3}^* & \cdots & \rho_{z,4M-1}^* \\ \rho_{z,2} & \rho_{z,1} & \rho_{z,2}^* & \cdots & \rho_{z,4M-2}^* \\ \rho_{z,3} & \rho_{z,2} & \rho_{z,1} & \ddots & \vdots \\ \vdots & \vdots & \ddots & \ddots & \rho_{z,2}^* \\ \rho_{z,4M-1} & \rho_{z,4M-2} & \cdots & \rho_{z,2} & \rho_{z,1} \end{bmatrix} \tag{6}$$

where $r_{z,ij}$ denotes the (i, j)-th element of the matrix $\mathbf{R}_z$ and is given by

$$r_{z,ij} = \sum\nolimits_{k=1}^{K} \sigma_{s,k}^2 a_z[i](\theta_k, r_k) a_z^*[j](\theta_k, r_k) + \sigma_n^2 \delta_{ij}, \quad 1 \le i,\ j \le 4M-1,\ 1 \le k \le K \tag{7}$$

where $a_z[i](\theta_k, r_k)$ is the i-th element of the vector $\mathbf{a}_z(\theta_k, r_k)$, $\sigma_{s,k}^2$ the power of the k-th source, and δ_{ij} the *Dirac delta* function. Equation (6) shows the relationship between $\rho_{z,i}$ and $r_{z,ij}$ as

$$\rho_{z,i} = r_{z,i1}, \quad 1 \le i \le 4M-1 \tag{8}$$

2.2. Data Model of the Cross Array Composed of the NLA

In this paper, a cross array composed of two NLA is designed to locate the 3D NF sources. The cross array consists of two symmetric NLA with $2M + 1$ sensors along Y and Z axis, respectively (Fig. 2). In each branch NLA, both $d(-M, -M+1)$ and $d(M-1, M)$ are equal to d, and $d(m, m+1)$, $m \in [-M+1, M-2]$ is equal to $2d$, where $d(m, m+1)$ is defined as the inter-sensor spacing between the m-th and $(m+1)$-th sensors. In Fig. 2, the red and blue *solid* circles denote

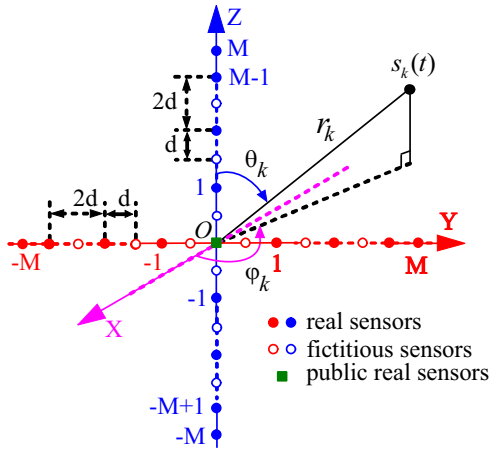

Figure 2. The array configuration structure.

the real sensors, the green *solid* square denotes the *public* real sensor between the NLAs at Z and Y axes, and the red and blue *hollow* circles denote the fictitious sensors (namely there is no sensor, and the output signal of the fictitious sensor is "zero").

Let the array center be phase reference point (see Fig. 2), the NLA output aligned with Z axis is given by

$$\bar{\mathbf{z}}(t) = \sum_{k=1}^{K} \bar{\mathbf{a}}_z(\theta_k, r_k) s_k(t) + \bar{n}_z(t) = \bar{\mathbf{A}}_z \mathbf{s}(t) + \bar{\mathbf{n}}_z(t) \tag{9}$$

where $\bar{\mathbf{z}}(t) = [\bar{z}_{-M}(t), \ldots, \bar{z}_0(t), \ldots, \bar{z}_M(t)]^T$ is a $(2M+1) \times 1$ complex vector from $2M+1$ sensors along Z axis, $\bar{\mathbf{n}}_z(t) = [\bar{n}_{z,-M}(t), \ldots, \bar{n}_{z,0}(t), \ldots, \bar{n}_{z,M}(t)]^T$ the array noise vector, and $\bar{\mathbf{a}}_z(\theta_k, r_k)$ the steering vector represented by $\bar{\mathbf{a}}_z(\theta_k, r_k) = [\bar{a}_{z,-M}(\theta_k, r_k), \ldots, \bar{a}_{z,0}(\theta_k, r_k), \ldots, \bar{a}_{z,M}(\theta_k, r_k)]^T$ with

$$\begin{aligned}
\bar{\mathbf{a}}_z(\theta_k, r_k) &= \bar{\mathbf{a}}_z(\varsigma_{z,k}, \xi_{z,k}) \\
&= \Big[e^{j[(-2M+1)\varsigma_{z,k} + (-2M+1)^2 \xi_{z,k}]}, e^{j[(-2M+2)\varsigma_{z,k} + (-2M+2)^2 \xi_{z,k}]}, \\
&\quad e^{j[(-2M+4)\varsigma_{z,k} + (-2M+4)^2 \xi_{z,k}]}, \ldots, e^{j[(-2)\varsigma_{z,k} + (-2)^2 \xi_{z,k}]}, \\
&\quad 1, e^{j[(2)\varsigma_{z,k} + (2)^2 \xi_{z,k}]}, \ldots, e^{j[(2M-4)\varsigma_{z,k} + (2M-4)^2 \xi_{z,k}]}, \\
&\quad e^{j[(2M-2)\varsigma_{z,k} + (2M-2)^2 \xi_{z,k}]}, e^{j[(2M-1)\varsigma_{z,k} + (2M-1)^2 \xi_{z,k}]} \Big]^T
\end{aligned} \tag{10}$$

and

$$\bar{\mathbf{A}}_z = [\bar{\mathbf{a}}_z(\varsigma_{z,1}, \xi_{z,1}), \bar{\mathbf{a}}_z(\varsigma_{z,2}, \xi_{z,2}), \ldots, \bar{\mathbf{a}}_z(\varsigma_{z,K}, \xi_{z,K})] \tag{11}$$

Similarly, the NLA output along Y axis can be expressed as

$$\mathbf{y}(t) = \sum_{k=1}^{K} \mathbf{a}_y(\theta_k, r_k, \varphi_k) s_k(t) + n_y(t) = \mathbf{A}_y \mathbf{s}(t) + \mathbf{n}_y(t) \tag{12}$$

where θ_k, r_k and φ_k denote the elevation angle, range and azimuth angle of k-th NF source, respectively. $\mathbf{y}(t)=[y_{-M}(t), \ldots, y_0(t), \ldots, y_M(t)]^T$ is a $(2M+1) \times 1$ complex vector from $2M+1$ sensors along Y axis, and $\mathbf{n}_y(t) = [n_{y,-M}(t), \ldots, n_{y,0}(t), \ldots, n_{y,M}(t)]^T$ is the array noise vector, and

$$\begin{aligned}
&\mathbf{a}_y(\theta_k,r_k,\varphi_k) = \mathbf{a}_y(\varsigma_{y,k}, \xi_{y,k}) \\
&= \Big[e^{j[(-2M+1)\varsigma_{y,k}+(-2M+1)^2\xi_{y,k}]}, e^{j[(-2M+2)\varsigma_{y,k}+(-2M+2)^2\xi_{y,k}]}, \\
&\quad e^{j[(-2M+4)\varsigma_{y,k}+(-2M+4)^2\xi_{y,k}]}, \ldots, e^{j[(-2)\varsigma_{y,k}+(-2)^2\xi_{y,k}]}, \\
&\quad 1, e^{j[(2)\varsigma_{y,k}+(2)^2\xi_{y,k}]}, \ldots, e^{j[(2M-4)\varsigma_{y,k}+(2M-4)^2\xi_{y,k}]}, \\
&\quad e^{j[(2M-2)\varsigma_{y,k}+(2M-2)^2\xi_{y,k}]}, e^{j[(2M-1)\varsigma_{y,k}+(2M-1)^2\xi_{y,k}]}\Big]^T
\end{aligned} \tag{13}$$

where

$$\varsigma_{y,k} = -\frac{2\pi d}{\lambda} \sin\theta_k \sin\varphi_k \tag{14}$$

$$\xi_{y,k} = \frac{\pi d^2}{\lambda r_k} \left(1 - \sin^2\theta_k \sin^2\varphi_k\right) \tag{15}$$

and

$$\mathbf{A}_y = [\mathbf{a}_y(\varsigma_{y,1}, \xi_{y,1}), \mathbf{a}_y(\varsigma_{y,2}, \xi_{y,2}), \ldots, \mathbf{a}_y(\varsigma_{y,K}, \xi_{y,K})] \tag{16}$$

The objective of this paper is to jointly estimate the elevation angle, range and azimuth angle $\{\theta_k, r_k, \varphi_k\}$ for $k = 1, \ldots, K$. Throughout the paper, the following hypotheses are assumed to hold:

1) The incoming source signals are statistically independent, zero-mean complex Gaussian random processes as [14–20]; 2) The noise is zero-mean, complex circular Gaussian, and spatially uniformly white, is statistically independent of all the signals and the noise variance is σ_n^2 as [14–20]; 3) For unique estimation of the bearing parameters, we require $d(M-1, M) = d(-M, -M+1) = d \leq \lambda/4$ and $d(m, m+1) = 2d \leq \lambda/2$ for $m \in [-M+1, M-2]$, which is different from the algorithms in [14–20]; 4) The number of sources satisfies $K \leq 2M-1$, which is also different from the algorithms in [14–20].

3. PROPOSED ALGORITHM

3.1. Array Aperture Extension

Firstly, we construct a new Hermitain Toeplitz matrix from the covariance matrix generated by the NLA with $2M+1$ sensors along Z axis.

Because the fictitious sensors (the sensors which are denoted by the red and blue hollow circles in Fig. 2) are virtually nonexistent, we assume that the output signal of each fictitious sensor is "zero". Thus, based on the real and fictitious sensors, a new vector $\bar{\mathbf{z}}'(t)$ can be constructed from $\bar{\mathbf{z}}(t)$ as

$$\begin{aligned}\bar{\mathbf{z}}'(t) &= \big[\bar{z}'_{-2M+1}(t), \bar{z}'_{-2M+2}(t), \bar{z}'_{-2M+3}(t), \ldots, \\ &\quad \bar{z}'_{-1}(t), \bar{z}'_{0}(t), \bar{z}'_{1}(t), \ldots, \bar{z}'_{2M-2}(t), \bar{z}'_{2M-1}(t)\big]^T \\ &= \big[\bar{z}_{-M}(t), \bar{z}_{-M+1}(t), 0, \bar{z}_{-M+2}(t), \ldots, \\ &\quad 0, \bar{z}_{0}(t), 0, \ldots, \bar{z}_{M-2}(t), 0, \bar{z}_{M-1}(t), \bar{z}_{M}(t)\big]^T \end{aligned} \tag{17}$$

It is noted that each 0 element in vector $\bar{\mathbf{z}}'(t)$ is one to one corresponding to each fictitious sensor.

Similar to the covariance matrix $\mathbf{R}_z$, the covariance matrix $\bar{\mathbf{R}}_z$ can be defined as

$$\begin{aligned}\bar{\mathbf{R}}_z &= \left(\bar{r}_{z,ij}\right) = E\left\{\bar{\mathbf{z}}'(t)\bar{\mathbf{z}}'^H(t)\right\} \\ &= \begin{bmatrix} \rho_{z,1} & \rho^*_{z,2} & 0 & \rho^*_{z,4} & \cdots & \rho^*_{z,4M-4} & 0 & \rho^*_{z,4M-2} & \rho^*_{z,4M-1} \\ \rho_{z,2} & \rho_{z,1} & 0 & \rho^*_{z,3} & \cdots & \rho^*_{z,4M-5} & 0 & \rho^*_{z,4M-3} & \rho^*_{z,4M-2} \\ 0 & 0 & 0 & 0 & \cdots & 0 & 0 & 0 & 0 \\ \rho_{z,4} & \rho_{z,3} & 0 & \rho_{z,1} & \cdots & \rho^*_{z,4M-7} & 0 & \rho^*_{z,4M-5} & \rho^*_{z,4M-4} \\ \vdots & \vdots & \vdots & \vdots & \ddots & \vdots & \vdots & \vdots & \vdots \\ \rho_{z,4M-4} & \rho_{z,4M-5} & 0 & \rho_{z,4M-7} & \cdots & \rho_{z,1} & 0 & \rho^*_{z,2} & \rho^*_{z,4} \\ 0 & 0 & 0 & 0 & \cdots & 0 & 0 & 0 & 0 \\ \rho_{z,4M-2} & \rho_{z,4M-3} & 0 & \rho_{z,4M-5} & \cdots & \rho_{z,3} & 0 & \rho_{z,1} & \rho^*_{z,2} \\ \rho_{z,4M-1} & \rho_{z,4M-2} & 0 & \rho_{z,4M-4} & \cdots & \rho_{z,4} & 0 & \rho_{z,2} & \rho_{z,1} \end{bmatrix} \end{aligned} \tag{18}$$

where $\bar{r}_{z,ij}$ denotes the (i,j)-th element of $\bar{\mathbf{R}}_z$.

From (18), we can observe that the matrix $\bar{\mathbf{R}}_z$ has not the Hermitain Toeplitz structure unlike $\mathbf{R}_z$, but at least one element is nonzero on its each diagonal line, which is paralleled to the main diagonal line, and each nonzero element on each diagonal line is equal to each other (Note that this result is determined by the structure of the array in Fig. 2 and is easy to be derived and validated). Meanwhile, from Equation (6), we can know that the matrix $\mathbf{R}_z$ has

$8M-1$ diagonal lines which are paralleled to the main diagonal line. Therefore, we can construct a Hermitain Toeplitz matrix [7] $\bar{\mathbf{R}}_{zT}$ from $\bar{\mathbf{R}}_z$

$$\bar{\mathbf{R}}_{zT} = \begin{bmatrix} \rho_{zT,1} & \rho^*_{zT,2} & \underline{\rho^*_{zT,3}} & \rho^*_{zT,4} & \cdots & \rho^*_{zT,4M-4} \\ \rho_{zT,2} & \rho_{zT,1} & \underline{\rho^*_{zT,2}} & \rho^*_{zT,3} & \cdots & \rho^*_{zT,4M-5} \\ \underline{\rho_{zT,3}} & \underline{\rho_{zT,2}} & \underline{\rho_{zT,1}} & \underline{\rho^*_{zT,2}} & \cdots & \underline{\rho^*_{zT,4M-6}} \\ \rho_{zT,4} & \rho_{zT,3} & \underline{\rho_{zT,2}} & \rho_{zT,1} & \cdots & \rho^*_{zT,4M-7} \\ \vdots & \vdots & \vdots & \vdots & \ddots & \vdots \\ \rho_{zT,4M-4} & \rho_{zT,4M-5} & \underline{\rho_{zT,4M-6}} & \rho_{zT,4M-7} & \cdots & \rho_{zT,1} \\ \underline{\rho_{zT,4M-3}} & \underline{\rho_{zT,4M-4}} & \underline{\rho_{zT,4M-5}} & \underline{\rho_{zT,4M-6}} & \cdots & \underline{\rho_{zT,2}} \\ \rho_{zT,4M-2} & \rho_{zT,4M-3} & \underline{\rho_{zT,4M-4}} & \rho_{zT,4M-5} & \cdots & \rho_{zT,3} \\ \rho_{zT,4M-1} & \rho_{zT,4M-2} & \underline{\rho_{zT,4M-3}} & \rho_{zT,4M-4} & \cdots & \rho_{zT,4} \end{bmatrix} \begin{bmatrix} \underline{\rho^*_{zT,4M-3}} & \rho^*_{zT,4M-2} & \rho^*_{zT,4M-1} \\ \underline{\rho^*_{zT,4M-4}} & \rho^*_{zT,4M-3} & \rho^*_{zT,4M-2} \\ \underline{\rho^*_{zT,4M-5}} & \underline{\rho^*_{zT,4M-4}} & \underline{\rho^*_{zT,4M-3}} \\ \underline{\rho^*_{zT,4M-6}} & \rho^*_{zT,4M-5} & \rho^*_{zT,4M-4} \\ \vdots & \vdots & \vdots \\ \underline{\rho^*_{zT,2}} & \rho^*_{zT,3} & \rho^*_{zT,4} \\ \underline{\rho_{zT,1}} & \underline{\rho^*_{zT,2}} & \underline{\rho^*_{zT,3}} \\ \underline{\rho_{zT,2}} & \rho_{zT,1} & \rho^*_{zT,2} \\ \underline{\rho_{zT,3}} & \rho_{zT,2} & \rho_{zT,1} \end{bmatrix} \tag{19}$$

and define $\rho_{zT,i}$ as

$$\rho_{zT,i} = \frac{1}{M_i} \sum_{n=i}^{4M-1} \bar{r}_{z,(n)(n+1-i)} = \rho_{z,i}, \quad 1 \le i \le 4M-1, \quad i \le n \le 4M-1 \tag{20}$$

where M_i is the number of nonzero elements on the i-th lower left diagonal line, which is paralleled to the main diagonal line, of the matrix $\bar{\mathbf{R}}_z$. Note that all zero elements of the covariance matrix $\bar{\mathbf{R}}_z$ are replaced with the corresponding to $\rho_{zT,i}$ or $\rho^*_{zT,i}$ (please see the element remarked by the underline in Equation (19)).

After comparing (6), (8) and (19), (20), one can easily find

$$\mathbf{R}_z = \bar{\mathbf{R}}_{zT} \tag{21}$$

and thus similar to (1), (21) can be obtained as

$$\begin{aligned} \mathbf{R}_z &= E\Big\{[\mathbf{A}_z\mathbf{s}(t) + \mathbf{n}_z(t)][\mathbf{A}_z\mathbf{s}(t) + \mathbf{n}_z(t)]^H\Big\} \\ &= \bar{\mathbf{R}}_{zT} = E\Big\{\big[\mathbf{A'}_z\mathbf{s}(t) + \mathbf{n'}_z(t)\big]\big[\mathbf{A'}_z\mathbf{s}(t) + \mathbf{n'}_z(t)\big]^H\Big\} \end{aligned} \tag{22}$$

From (22), one can easily obtain the following results:

$$\begin{aligned}\mathbf{A}'_z &= \left[\mathbf{a}'_z(\theta_1, r_1), \mathbf{a}'_z(\theta_2, r_2), \ldots, \mathbf{a}'_z(\theta_K, r_K)\right] \\ &= \left[\mathbf{a}_z(\theta_1, r_1), \mathbf{a}_z(\theta_2, r_2), \ldots, \mathbf{a}_z(\theta_K, r_K)\right] = \mathbf{A}_z \qquad (23) \\ &\quad \mathbf{a}'_z(\varsigma_{z,k}, \xi_{z,k}) \\ &= \Big[e^{j[(-2M+1)\varsigma_{z,k}+(-2M+1)^2\xi_{z,k}]}, e^{j[(-2M+2)\varsigma_{z,k}+(-2M+2)^2\xi_{z,k}]}, \\ &\quad e^{j[(-2M+3)\varsigma_{z,k}+(-2M+3)^2\xi_{z,k}]}, \ldots, e^{j[m\varsigma_{z,k}+m^2\xi_{z,k}]}, \ldots, \\ &\quad e^{j[(2M-2)\varsigma_{z,k}+(2M-2)^2\xi_{z,k}]}, e^{j[(2M-1)\varsigma_{z,k}+(2M-1)^2\xi_{z,k}]}\Big]^T \\ &= \mathbf{a}_z(\varsigma_{z,k}, \xi_{z,k}) = \mathbf{a}_z(\theta_k, r_k) \qquad (24)\end{aligned}$$

$$\mathbf{n}'_z(t) = \left[n'_{z,-2M+1}(t), \ldots, n'_{z,0}(t), \ldots, n'_{z,2M-1}(t)\right]^T = \mathbf{n}_z(t) \qquad (25)$$

Therefore, we can know from Equations (22)–(25) that the new matrix $\bar{\mathbf{R}}_{zT}$ generated by the NLA with $2M+1$ sensors along Z axis is equivalent to the covariance matrix $\mathbf{R}_z$ generated by the ULA with $4M-1$ sensors along Z axis; in other words, the constructed matrix $\bar{\mathbf{R}}_{zT}$ which is from a NLA with $2M+1$ sensors along Z axis can be considered as the covariance matrix generated by a ULA with $4M-1$ sensors along Z axis.

Then, we construct another new Hermitain Toeplitz matrix from the covariance matrix by generated by the NLA with $2M+1$ sensors along Y axis.

Similar to the constructed procedure of the matrix $\bar{\mathbf{R}}_{zT}$, based on the NLA with $2M+1$ sensors along Y axis, we first construct a new vector $\bar{\mathbf{y}}'(t)$ from $\mathbf{y}(t)$ as

$$\begin{aligned}\bar{\mathbf{y}}'(t) &= \left[\bar{y}'_{-2M+1}(t), \bar{y}'_{-2M+2}(t), \bar{y}'_{-2M+3}(t), \ldots,\right. \\ &\quad \left.\bar{y}'_{-1}(t), \bar{y}'_0(t), \bar{y}'_1(t), \ldots, \bar{y}'_{2M-2}(t), \bar{y}'_{2M-1}(t)\right]^T \\ &= \left[y_{-M}(t), y_{-M+1}(t), 0, y_{-M+2}(t), \ldots, 0, y_0(t), 0,\right. \\ &\quad \left.\ldots, y_{M-2}(t), 0, y_{M-1}(t), y_M(t)\right]^T \qquad (26)\end{aligned}$$

And, the covariance matrix $\bar{\mathbf{R}}_y$ can be defined as

$$\bar{\mathbf{R}}_y = (\bar{r}_{y,ij}) = E\left\{\bar{\mathbf{y}}'(t)\bar{\mathbf{y}}'^H(t)\right\} \qquad (27)$$

where $\bar{r}_{y,ij}$ denotes the (i,j)-th element of the matrix $\bar{\mathbf{R}}_y$.

As the matrix $\bar{\mathbf{R}}_z$, $\bar{\mathbf{R}}_y$ has also not the Hermitain Toeplitz structure, and thus similar to the constructed procedure of $\bar{\mathbf{R}}_{zT}$, we

can construct a Hermitain Toeplitz matrix $\bar{\mathbf{R}}_{yT}$ from $\bar{\mathbf{R}}_y$ as

$$\bar{\mathbf{R}}_{yT} = \begin{bmatrix} \rho_{y,1} & \rho_{y,2}^* & \rho_{y,3}^* & \cdots & \rho_{y,4M-1}^* \\ \rho_{y,2} & \rho_{y,1} & \rho_{y,2}^* & \cdots & \rho_{y,4M-2}^* \\ \rho_{y,3} & \rho_{y,2} & \rho_{y,1} & \ddots & \vdots \\ \vdots & \vdots & \ddots & \ddots & \rho_{y,2}^* \\ \rho_{y,4M-1} & \rho_{y,4M-2} & \cdots & \rho_{y,2} & \rho_{y,1} \end{bmatrix} \tag{28}$$

As (21), one easily find

$$\begin{aligned} \mathbf{R}_y &= E\Big\{\mathbf{y}(t)\mathbf{y}^H(t)\Big\} = E\Big\{[\mathbf{A}_y\mathbf{s}(t)+\mathbf{n}_y(t)][\mathbf{A}_y\mathbf{s}(t)+\mathbf{n}_y(t)]^H\Big\} \\ &= \bar{\mathbf{R}}_{yT} = E\Big\{[\mathbf{A'}_y\mathbf{s}(t)+\mathbf{n'}_y(t)][\mathbf{A'}_y\mathbf{s}(t)+\mathbf{n'}_y(t)]^H\Big\} \end{aligned} \tag{29}$$

where

$$\begin{aligned} \mathbf{A'}_y &= \left[\mathbf{a'}_y(\theta_1, r_1, \varphi_1), \mathbf{a'}_y(\theta_2, r_2, \varphi_2), \ldots, \mathbf{a'}_y(\theta_K, r_K, \varphi_K)\right] \\ &= \left[\mathbf{a'}_y(\varsigma_{y,1}, \xi_{y,1}), \mathbf{a'}_y(\varsigma_{y,2}, \xi_{y,2}), \ldots, \mathbf{a'}_y(\varsigma_{y,K}, \xi_{y,K})\right] = \mathbf{A}_y \quad (30) \\ &\quad \mathbf{a'}_y(\varsigma_{y,k}, \xi_{y,k}) \\ &= \Big[e^{j[(-2M+1)\varsigma_{y,k}+(-2M+1)^2\xi_{y,k}]}, e^{j[(-2M+2)\varsigma_{y,k}+(-2M+2)^2\xi_{y,k}]}, \\ &\quad e^{j[(-2M+3)\varsigma_{y,k}+(-2M+3)^2\xi_{y,k}]}, \ldots, e^{j[m\varsigma_{y,k}+m^2\xi_{y,k}]}, \ldots, \\ &\quad e^{j[(2M-2)\varsigma_{y,k}+(2M-2)^2\xi_{y,k}]}, e^{j[(2M-1)\varsigma_{y,k}+(2M-1)^2\xi_{y,k}]}\Big]^T \\ &= \mathbf{a}_y(\varsigma_{y,k}, \xi_{y,k}) \quad (31) \\ \mathbf{n'}_y(t) &= \left[n'_{y,-2M+1}(t), \ldots, n'_{y,0}(t), \ldots, n'_{y,2M-1}(t)\right]^T = \mathbf{n}_y(t) \quad (32) \end{aligned}$$

Likewise, similar to the constructed matrix $\bar{\mathbf{R}}_{zT}$, the constructed matrix $\bar{\mathbf{R}}_{yT}$ which is from a NLA with $2M+1$ sensors along Y axis can be considered as the covariance matrix generated by a ULA with $4M-1$ sensors along Y axis.

3.2. Elevation Angle Estimation

Based on (6) and (7), the anti-diagonal elements of $\bar{\mathbf{R}}_{zT}$ (Note that $\mathbf{R}_z = \bar{\mathbf{R}}_{zT}$ has been proved above) can be given [16] by

$$r_{i,4M-i} = \sum_{k=1}^{K} \sigma_{s,k}^2 e^{-j2(2M-i)\varsigma_{z,k}} + \sigma_n^2 \delta_{i,4M-i}, \quad i = 1, 2, \ldots, 4M-1 \tag{33}$$

Hence, from (33) we can form a $(4M-1)\times 1$ vector $\mathbf{x}$ for all $i = 1, 2, \ldots, 4M-1$ as

$$\mathbf{x} = \Big[x(-2M+1), x(-2M+2), \ldots, x(-1), x(0),$$

$$
\begin{aligned}
& x(1), \ldots, x(2M-2), x(2M-1)\Big]^T \\
= & \left[\sum_{k=1}^{K} \sigma_{sk}^2 e^{-j(2M-1)\bar{\varsigma}_{z,k}}, \ldots, \sum_{k=1}^{K} \sigma_{sk}^2 e^{-j\bar{\varsigma}_{z,k}}, \sum_{k=1}^{K} \sigma_{sk}^2 \right. \\
& \left. + \sigma_n^2, \sum_{k=1}^{K} \sigma_{sk}^2 e^{j\bar{\varsigma}_{z,k}}, \ldots, \sum_{k=1}^{K} \sigma_{sk}^2 e^{j(2M-1)\bar{\varsigma}_{z,k}} \right]^T \qquad (34)
\end{aligned}
$$

where $x(i)$ is i-th element of the vector $\mathbf{x}$ and $\bar{\varsigma}_{z,k} = 2\varsigma_{z,k}$. Note that it is easy to find that the vector $\mathbf{x}$ only contains the elevation angle information. Next, we divide the vector $\mathbf{x}$ into two subvectors $\mathbf{x}_1$ and $\mathbf{x}_2$.

$$
\begin{aligned}
\mathbf{x}_1 &= [x_1(0), x_1(1), \ldots, x_1(2M-1)]^T \\
&= \left[\sum_{k=1}^{K} \sigma_{s,k}^2 + \sigma_n^2, \sum_{k=1}^{K} \sigma_{s,k}^2 e^{j\bar{\varsigma}_{z,k}}, \ldots, \sum_{k=1}^{K} \sigma_{s,k}^2 e^{j(2M-1)\bar{\varsigma}_{z,k}}\right]^T \qquad (35) \\
\mathbf{x}_2 &= [x_2(-2M+1), \ldots, x_2(-1), x_2(0)]^T \\
&= \left[\sum_{k=1}^{K} \sigma_{s,k}^2 e^{-j(2M+1)\bar{\varsigma}_{z,k}}, \ldots, \sum_{k=1}^{K} \sigma_{s,k}^2 e^{-j\bar{\varsigma}_{z,k}}, \sum_{k=1}^{K} \sigma_{s,k}^2 + \sigma_n^2\right]^T \qquad (36)
\end{aligned}
$$

where $x_1(i)$ and $x_2(i)$ denote the i-th element of the vectors $\mathbf{x}_1$ and $\mathbf{x}_2$, respectively.

We construct a $2M \times 2M$ Toeplitz matrix $\mathbf{R}_{\mathbf{x}_1}$ whose first column and row are $\mathbf{x}_1$ and $\mathbf{x}_1^H$, respectively

$$
\mathbf{R}_{\mathbf{x}_1} = \begin{bmatrix} x_1(0) & x_1^*(1) & \ldots & x_1^*(2M-1) \\ x_1(1) & x_1(0) & \ddots & \vdots \\ \vdots & \ldots & \ddots & x_1^*(1) \\ x_1(2M-1) & \ldots & x_1(1) & x_1(0) \end{bmatrix} = \mathbf{B}\mathbf{R}_{\mathbf{S}}\mathbf{B}^H + \bar{\mathbf{N}} \qquad (37)
$$

and based on Equation (35), we have

$$
\begin{aligned}
\mathbf{B} &= \left[\mathbf{b}(\bar{\varsigma}_{z,1}), \mathbf{b}(\bar{\varsigma}_{z,2}), \ldots, \mathbf{b}(\bar{\varsigma}_{z,K})\right] \qquad (38) \\
\mathbf{b}(\bar{\varsigma}_{z,k}) &= \left[1, e^{j\bar{\varsigma}_{z,k}}, \ldots, e^{j(2M-1)\bar{\varsigma}_{z,k}}\right]^T \qquad (39) \\
\mathbf{R}_{\mathbf{S}} &= E\Big\{\mathbf{s}(t)\mathbf{s}^H(t)\Big\} \qquad (40) \\
\bar{\mathbf{N}} &= \mathrm{diag}\Big\{\sigma_n^2, 0, \ldots, 0\Big\} \qquad (41)
\end{aligned}
$$

Likewise, we construct another $2M \times 2M$ Toeplitz matrix $\mathbf{R}_{\mathbf{x}_2}$

whose first column and row are $\mathbf{x}_2$ and $\mathbf{x}_2^H$ in reverse order, respectively

$$\mathbf{R}_{\mathbf{x}_2} = \begin{bmatrix} x_2(0) & x_2(-1) & \dots & x_2(-2M+1) \\ x_2^*(-1) & x_2(0) & \ddots & \vdots \\ \vdots & \dots & \ddots & x_2(-1) \\ x_2^*(-2M+1) & \dots & x_2^*(-1) & x_2(0) \end{bmatrix} \tag{42}$$

According to Equations (35) and (36) and comparing Equations (37) and (42), one can find that the matrix $\mathbf{R}_{\mathbf{x}_2}$ also satisfies $\mathbf{R}_{\mathbf{x}_2} = \mathbf{B}\mathbf{R}_{\mathbf{S}}\mathbf{B}^H + \bar{\mathbf{N}}$ as $\mathbf{R}_{\mathbf{x}_1} = \mathbf{B}\mathbf{R}_{\mathbf{S}}\mathbf{B}^H + \bar{\mathbf{N}}$, which shows that $\mathbf{R}_{\mathbf{x}_1}$ and $\mathbf{R}_{\mathbf{x}_2}$ are identical

$$\mathbf{R}_{\mathbf{x}_1} = \mathbf{R}_{\mathbf{x}_2} \tag{43}$$

Further, we can obtain the eigenvalue decomposition of $\mathbf{R}_{\mathbf{x}_1}$ or $\mathbf{R}_{\mathbf{x}_2}$ as

$$\begin{aligned} \mathbf{R}_{\mathbf{x}_1} &= \mathbf{R}_{\mathbf{x}_2} = \mathbf{U}\mathbf{\Lambda}\mathbf{U}^H = \mathbf{U}_s\mathbf{\Lambda}_s\mathbf{U}_s^H + \mathbf{U}_n\mathbf{\Lambda}_n\mathbf{U}_n^H \\ &= [\mathbf{u}_1, \dots, \mathbf{u}_{2M}]\mathrm{diag}\{\lambda_1, \dots, \lambda_{2M}\}[\mathbf{u}_1, \dots, \mathbf{u}_{2M}]^H \end{aligned} \tag{44}$$

where $\mathbf{\Lambda}$ is the diagonal matrix with the eigenvlues arranged as $\lambda_1 \geq \dots \geq \lambda_K \geq \lambda_{K+1} = \dots = \lambda_{2M}$; the $K \times K$ diagonal matrix $\mathbf{\Lambda}_s$ is composed of eigenvalues $\lambda_1, \dots, \lambda_K$; the $2M \times K$ matrix $\mathbf{U}_s$, which spans the signal subspace of $\mathbf{R}_{\mathbf{x}_1}$ or $\mathbf{R}_{\mathbf{x}_2}$, consists of the eigenvectors related to $\mathbf{u}_1, \dots, \mathbf{u}_K$. Similarly, the $(2M-K)\times(2M-K)$ diagonal matrix $\mathbf{\Lambda}_n$ is composed of eigenvalues $\lambda_{K+1}, \dots, \lambda_{2M}$, and the $(2M) \times (2M-K)$ matrix $\mathbf{U}_n$ consists of the eigenvectors related to $\mathbf{u}_{K+1}, \dots, \mathbf{u}_{2M}$, spanning the noise subspace of $\mathbf{R}_{\mathbf{x}_1}$ or $\mathbf{R}_{\mathbf{x}_2}$.

Note that it can be seen from the matrixes $\mathbf{R}_{\mathbf{x}_1}$ and $\mathbf{R}_{\mathbf{x}_2}$ that the diagonal matrix $\bar{\mathbf{N}}$ will not affect the eigenvalue decomposition of $\mathbf{R}_{\mathbf{x}_1}$ or $\mathbf{R}_{\mathbf{x}_2}$.

Finally, the elevation angles of the NF sources can be obtained by finding the K peaks from the following 1D spectrum function:

$$P(\bar{\varsigma}_z) = 1 \Big/ \left[\mathbf{b}^H(\bar{\varsigma}_z)\mathbf{U}_n\mathbf{U}_n^H\mathbf{b}(\bar{\varsigma}_z)\right] \tag{45}$$

By means of only 1D search over θ, the estimates $\hat{\theta}_k = \arccos(-\lambda\hat{\varsigma}_{z,k}/(2\pi d))$, $k = 1, \dots, K$ of the elevation angles θ_k, $k = 1, \dots, K$ corresponding to the estimates $\hat{\varsigma}_{z,k}$, $k = 1, \dots, K$ of all NF sources can be obtained.

Note that the elevation angles estimation of the multiple NF sources can be implemented through only once 1D search.

3.3. Range Estimation

It can be observed from (24) that virtual steering vector $\mathbf{a}'_z(\varsigma_{z,k}, \xi_{z,k})$ can be written into another form as:

$$\mathbf{a}'_z(\varsigma_{z,k}, \xi_{z,k}) = \mathbf{a}'_{z,1}(\varsigma_{z,k})\mathbf{a}'_{z,2}(\xi_{z,k}) \tag{46}$$

where $\mathbf{a}'_{z,1}(\varsigma_{z,k})$ is a $(4M-1)\times(2M)$ matrix and only contains the elevation angle parameters information.

$$\mathbf{a}'_{z,1}(\varsigma_{z,k}) = \begin{bmatrix} e^{j(-2M+1)\varsigma_{z,k}} & 0 & \cdots & 0 \\ 0 & e^{j(-2M+2)\varsigma_{z,k}} & \ddots & \vdots \\ \vdots & 0 & \ddots & 0 \\ 0 & \cdots & 0 & 1 \\ \vdots & 0 & \iddots & 0 \\ 0 & e^{j(2M-2)\varsigma_{z,k}} & \iddots & \vdots \\ e^{j(2M-1)\varsigma_{z,k}} & 0 & \cdots & 0 \end{bmatrix} \tag{47}$$

$\mathbf{a}'_{z,2}(\xi_{z,k})$ is a $2M\times 1$ matrix and contains the azimuth angle and range parameters information.

$$\mathbf{a}'_{z,2}(\xi_{z,k}) = \left[e^{j(-2M+1)^2\xi_{z,k}}, e^{j(-2M+2)^2\xi_{z,k}}, \ldots, 1\right]^T \tag{48}$$

To estimate $\xi_{z,k}$, similar to (44), we eigendecompose $\bar{\mathbf{R}}_{zT}$ to construct the $(4M-1)\times(4M-1-K)$ noise-subspace matrix $\bar{\mathbf{U}}_n$, whose columns are the $(4M-1)\times 1$ eigenvectors associated with the $(4M-1-K)$ smallest eigenvalues of $\bar{\mathbf{R}}_{zT}$.

Based on the conventional MUSIC algorithm and substituting estimates $\hat{\varsigma}_{z,k}$ into (24) (Equation (24) is equal to Equation (2)) we can find the minima of the following function:

$$\begin{aligned} \hat{\xi}_{z,k} &\triangleq \min_{\xi_z}\left\{\mathbf{a}'^H_z(\hat{\varsigma}_{z,k}, \xi_z)\bar{\mathbf{U}}_n\bar{\mathbf{U}}_n^H\mathbf{a}'_z(\hat{\varsigma}_{z,k}, \xi_z)\right\} \\ &= \min_{\xi_z}\left\{\mathbf{a}'^H_{z,2}(\xi_z)\mathbf{a}'^H_{z,1}(\hat{\varsigma}_{z,k})\bar{\mathbf{U}}_n\bar{\mathbf{U}}_n^H\mathbf{a}'_{z,1}(\hat{\varsigma}_{z,k})\mathbf{a}'_{z,2}(\xi_z)\right\} \end{aligned} \tag{49}$$

the minimal value of which indicates estimation $\hat{\xi}_{z,k}$. To avoid such a search in (49), we derive the following method.

Note that in fact, (49) implies that $\mathbf{a}'_{z,2}(\xi_{z,k})$ is the eigenvector corresponding to the smallest eigenvalue of Hermitian matrix $\mathbf{a}'^H_{z,1}(\hat{\varsigma}_{z,k})\bar{\mathbf{U}}_n\bar{\mathbf{U}}_n^H\mathbf{a}'_{z,1}(\hat{\varsigma}_{z,k})$ [9]. Therefore, based on the eigenvector $\mathbf{a}'_{z,2}(\xi_{z,k})$ obtained from the eigenvalue decomposition of $\mathbf{a}'^H_{z,1}(\hat{\varsigma}_{z,k})\bar{\mathbf{U}}_n\bar{\mathbf{U}}_n^H\mathbf{a}'_{z,1}(\hat{\varsigma}_{z,k})$, we define a $(2M-2)$-dimensional vector

$\mathbf{e}$, the i-th element of which has the following form:

$$\mathbf{e}(i) = \frac{\left(\mathbf{a'}_{z,2}(\hat{\xi}_{z,k})[2M-i]\right)\cdot\left(\mathbf{a'}_{z,2}\left(\hat{\xi}_{z,k}\right)[2M]\right)}{\left(\mathbf{a'}_{z,2}\left(\hat{\xi}_{z,k}\right)[2M+1-i]\right)\cdot\left(\mathbf{a'}_{z,2}\left(\hat{\xi}_{z,k}\right)[2M-1]\right)} = e^{j2(i-1)\hat{\xi}_{z,k}}, \quad i=1,\ldots,2M-2 \tag{50}$$

where $\mathbf{a'}_{z,2}(\hat{\xi}_{z,k})[2M-1]$ denotes the $(2M-1)$-th element of $\mathbf{a'}_{z,2}(\hat{\xi}_{z,k})$. From (49), $\hat{\xi}_{z,k}$ can be easily obtained as follows:

$$\hat{\xi}_{z,k} = \frac{1}{2(2M-3)}\sum_{i=1}^{2M-3}\arg\left(\frac{\mathbf{e}(i+1)}{\mathbf{e}(i)}\right) \tag{51}$$

3.4. Azimuth Angle Estimation

We can see from (29) and (30) that $\bar{\mathbf{R}}_{yT}$ contains 3D parameters, namely elevation/azimuth angles and range.

Since the constructed matrix $\bar{\mathbf{R}}_{yT}$, which is from a NLA with $2M+1$ sensors along Y axis, can be considered as the covariance matrix generated by a ULA with $4M-1$ sensors along Y axis, thus the eigendecomposition of the constructed matrix $\bar{\mathbf{R}}_{yT}$ can be written as

$$\bar{\mathbf{R}}_{yT} = \mathbf{E}_s\Omega_s\mathbf{E}_s^H + \mathbf{E}_n\Omega_n\mathbf{E}_n^H \tag{52}$$

where Ω_s and Ω_n are the diagonal matrices that contain the signal- and noise-subspace eigenvalues of $\bar{\mathbf{R}}_{yT}$, respectively, whereas $\mathbf{E}_s$ and $\mathbf{E}_n$ are the orthonormal matrices that contain the signal- and noise-subspace eigenvectors of $\bar{\mathbf{R}}_{yT}$, respectively. Based on the MUSIC method and (31), a 3D MUSIC spectrum function is given by:

$$P(\theta,r,\varphi) = 1\Big/\left[\mathbf{a'}_y^H(\theta,r,\varphi)\mathbf{E}_n\mathbf{E}_n^H\mathbf{a'}_y(\theta,r,\varphi)\right] \tag{53}$$

With the elevation angle and range estimates $\{\hat{\theta}_k, \hat{r}_k\}$, $k = 1, \ldots, K$, (53) can be rewritten as

$$P(\varphi) = 1/[\mathbf{a'}_y^H(\hat{\theta}_k,\varphi,\hat{r}_k)\mathbf{E}_n\mathbf{E}_n^H\mathbf{a'}_y(\hat{\theta}_k,\varphi,\hat{r}_k)], \quad k=1,\ldots,K \tag{54}$$

By means of 1D search over φ, the estimates $\hat{\varphi}_k$, $k = 1, \ldots, K$ of the azimuth angles φ_k, $k = 1, \ldots, K$ of all NF sources can be obtained.

3.5. Summary of the Proposed Algorithm

The proposed algorithm can be described as follows:

Step 1: Construct $(4M-1)\times 1$ output vector $\bar{\mathbf{z}}'(t)$ from $(2M+1)\times 1$ output vector $\bar{\mathbf{z}}(t)$ and then obtain the $(4M-1)\times(4M-1)$ covariance matrix $\bar{\mathbf{R}}_z$. Based on (18) and $\bar{\mathbf{R}}_{\bar{z}}$, construct the $(4M-1)\times(4M-1)$ Hermitain Toeplitz matrix $\bar{\mathbf{R}}_{zT}$. Meanwhile, in the same method, construct the $(4M-1)\times(4M-1)$ Hermitain Toeplitz matrix $\bar{\mathbf{R}}_{yT}$;

Step 2: Construct one Toeplitz matrix $\mathbf{R}_{\mathbf{x}_1}$ or $\mathbf{R}_{\mathbf{x}_2}$, and then implement the eigenvalue decomposition of $\mathbf{R}_{\mathbf{x}_1}$ or $\mathbf{R}_{\mathbf{x}_2}$ to obtain its noise subspace $\mathbf{U}_n$;

Step 3: Based on the MUSIC method, obtain the estimates $\hat{\theta}_k$, $k=1,\ldots,K$ of the elevation angles θ_k, $k=1,\ldots,K$ of all NF sources from $\hat{\theta}_k=\arccos[-\hat{\varsigma}_{z,k}\lambda/(2\pi d)]$.

Step 4: Implement the eigenvalue decomposition of $\bar{\mathbf{R}}_{zT}$ to obtain its noise subspace $\bar{\mathbf{U}}_n$, and substitute the estimates $\hat{\varsigma}_{z,k}$ into $\mathbf{a}_z(\varsigma_{z,k},\xi_{z,k})$ so as to form Hermitian matrix $\mathbf{a}_{z,1}^H(\hat{\varsigma}_{z,k})\bar{\mathbf{U}}_n\bar{\mathbf{U}}_n^H\mathbf{a}_{z,1}(\hat{\varsigma}_{z,k})$;

Step 5: Implement the eigenvalue decomposition of $\mathbf{a}_{z,1}^H(\hat{\varsigma}_{z,k})\bar{\mathbf{U}}_n\bar{\mathbf{U}}_n^H\mathbf{a}_{z,1}(\hat{\varsigma}_{z,k})$ to obtain the eigenvector corresponding to the smallest eigenvalue, i.e., $\mathbf{a}_{z,2}(\hat{\xi}_{z,k})$;

Step 6: Estimate $\hat{\xi}_{z,k}$ from (51), and obtain the estimates $\hat{r}_k$, $k=1,\ldots,K$ of the ranges r_k, $k=1,\ldots,K$ of all NF sources from $\hat{r}_k=[\pi d^2\sin^2(\hat{\theta}_k)]/(\lambda\hat{\xi}_{z,k})$.

Step 7: Implement the eigenvalue decomposition of $\bar{\mathbf{R}}_{yT}$ to obtain its noise subspace $\mathbf{E}_n$. And then with the elevation angle and range estimates $\{\hat{\theta}_k,\hat{r}_k\}$, $k=1,\ldots,K$ and based on 1D search MUSIC method, obtain the azimuth angle estimates $\hat{\varphi}_k$, $k=1,\ldots,K$.

3.6. Discussion

In this Section, we analyze the performance of the proposed algorithm in four aspects: **Array aperture**, **Parameter pairing**, **Computational Complexity** and **Estimation Accuracy**.

3.6.1. Array Aperture

According to the subspace theory [2, 3], the number of sources to be processed must be less than the minimal value between the number of rows and that of columns of the constructed matrix. The methods addressed in [14, 15] can construct $(M+1)\times(M+1)$-dimensional matrix using a ULA of $2M+2$ sensors, and the algorithms addressed in [16, 17, 20] can construct $(M+1)\times(M+1)$-dimensional matrix

with a ULA of $2M+1$ sensors, whereas the proposed algorithm can construct $2M \times 2M$-dimensional matrix $\mathbf{R}_{\mathbf{x}_1}$ or $\mathbf{R}_{\mathbf{x}_2}$ using a NLA of $2M+1$ sensors. Therefore, when considering the number of sources to be processed, the methods in [14, 15] can locate at most M sources using a ULA of $2M+2$ sensors, and the algorithms in [16, 17, 20] can locate at most M sources with a ULA of $2M+1$ sensors, however, the proposed algorithm is able to locate $2M-1$ using a NLA of $2M+1$ sensors. The analysis above indicates that the proposed algorithm has larger array aperture than the algorithms in [14–17, 20].

3.6.2. Parameter Pairing

Many 2D [14–17] and 3D [18–20] NF sources estimation algorithms need to pair parameters so as to achieve the source localization. However, the failure in pairing will cause severe performance degradation. In this paper, the proposed algorithm first estimates the elevation angle $\hat{\theta}_k$, then with the elevation angle estimate $\hat{\theta}_k$ obtains the range estimate $\hat{r}_k$, and last achieves the estimation of azimuth angle $\hat{\varphi}_k$ with the estimate $\{\hat{\theta}_k, \hat{r}_k\}$. Therefore, the proposed algorithm avoids parameter match operation and extra computational load for the parameters match procedure.

3.6.3. Computational Complexity

In this discussion, we only consider the major computations. Although these algorithms in [13, 21, 22, 25] also have not parameters match procedure, these algorithms have large amount of computational cost for the high-dimensional search or complex iterative process. More specifically, the algorithm in [13] needs to perform 2D search process for localizing the 2D NF sources, the algorithms in [21, 22] performs 3D search process for localizing the 3D NF sources, and the algorithm in [25] requires complex iterative procedure. However, the proposed algorithm needs to form two $(4M-1)\times(4M-1)$ covariance matrixes for Z and Y axes respectively, to construct two $(4M-1)\times(4M-1)$ Toeplitz matrixes for Z and Y axes respectively, to perform eigendecomposition of the Toeplitz matrix, and to execute once one-dimensional search for the elevation angle estimation. Then the proposed algorithm utilizes a free-search method to estimate the range parameters, and at last executes only 1D search to obtain the estimates of azimuth angle. Therefore, the proposed algorithm has a low computational load.

3.6.4. Estimation Accuracy and Resolution

On the one hand, based on the virtual cross-correlation computer theory [26], the estimation accuracy increases as the number of virtual sensors increases. The number of virtual sensors formed in [20] and that of the proposed algorithm are $M+1$ and $2M+1$, respectively. Therefore, the proposed algorithm is expected to obtain better estimation performance than [20]. On the other hand, when the number of sensors are $2M+1$, the array aperture of the algorithms in [14–20] is $D = (2M+1-1) \times \lambda/4 = M\lambda/2$, however the array aperture of the proposed algorithm is $D = (4M-2) \times \lambda/4 = M\lambda - \lambda/2$. Since $(M\lambda - \lambda/2) > M\lambda/2$ when $M > 1$, therefore, the proposed algorithm has larger array aperture than the algorithms in [14–20], which indicates that the proposed algorithm is expected to have better parameter estimation resolution than the algorithms in [23, 24].

4. SIMULATIONS

In this Section, to verify the performance of the proposed algorithm, various typical numerical experiments are performed. In the conventional classical 3D NF localization algorithms [18–25], the algorithms in [18, 19] are developed to deal with *non-Gaussian* sources, the algorithms in [21, 22, 25] are based on the complex high-dimensional search or iterative process, and the algorithms in [23, 24] are based on a special Y-shape and circular shape array, respectively; however the algorithm in [20] is developed to deal with the *Gaussian* sources based on the *cross array* and *SOS* just like the proposed algorithm. Therefore, in this paper, we choose the proximal 3D NF source localization algorithm proposed in [20] to compare the parameter estimation performance with the proposed algorithm.

We consider a cross array placed in the Y-Z plane, and each NLA branch (see Fig. 2) consists of 9 ($M = 4$) omnidirectional sensors with $d = \lambda/4$. The input signal-to-noise ratio (SNR) of the k-th source is defined as $10\log_{10}(\sigma_k^2/\sigma_n^2)$. The parameter estimation performance of the proposed algorithm and the algorithm in [20] is compared in terms of the root mean square error (RMSE) [25, 29], and the RMSE of the k-th signal source is defined by $\text{RMSE} = \sqrt{(1/Q)\sum_{q=1}^{Q}(\hat{\partial}_k^{(q)} - \partial_k)^2}$, where Q is the number of independent Metropolis-Hastings Monte Carlo [29, 30] trials and $\hat{\partial}_k^{(q)}$ denotes the estimates of the parameter ∂_k (∂_k can denotes the elevation angle, range or azimuth angle) of the k-th source in the q-th trial. Monte Carlo method is algorithm for solving various kinds of computational problems by using random numbers. Because of the repetitive nature of a typical Monte Carlo algorithm,

as well as the large number of calculations involved, the Monte Carlo method is particularly suited to calculation using a computer [29, 30]. In the following each experiment, the elevation/azimuth angle and range RMSE of the proposed algorithm and the algorithm in [20] is derived from 500 independent trials. Note that the algorithm in [20] uses a cross array placed in the X-Y plane, and each **ULA** branch consists of $2M+1 = 9$ omnidirectional sensors with inter-sensor spacing $\lambda/4$. And thus, the *Fresnel* zone (NF zone) of [20] is $(1.75\lambda, 8\lambda)$and that of the proposed algorithm is $(4.05\lambda, 24.5\lambda)$.

4.1. Parameter Estimation Performance

In the first experiment, we investigate the change of the RMSE of the estimated parameter as the SNR changes. Without loss of generality, two NF sources case is considered. The two NF sources are located at $\{\theta_1 = 40°, r_1 = 5\lambda, \varphi_1 = 80°\}$ and $\{\theta_2 = 60°, r_2 = 5.8\lambda, \varphi_2 = 50°\}$, respectively. The SNR varies from -5 dB to 25 dB, and the number of snapshots is fixed at 1000. We can note from Figs. 3, 4 and 5 that the proposed algorithm outperforms the algorithm in [20] in elevation angle, range and azimuth angle estimates, which is because that the proposed algorithm has larger array aperture and is able to locate more sources than the algorithm in [20] as the analysis in Section 3.6. Further, from Fig. 4, it can be seen that the range estimation accuracy for the first source, which is closer to the array, is higher than that of the second source, which is consistent with the analysis results in [14]. Moreover, from Figs. 3, 4 and 5, we can find that the

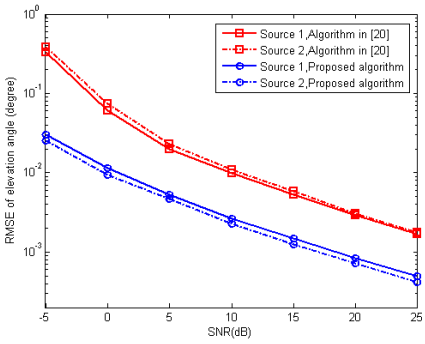

Figure 3. The RMSE of elevation angle estimates of both the algorithm in [20] and proposed algorithm versus SNR.

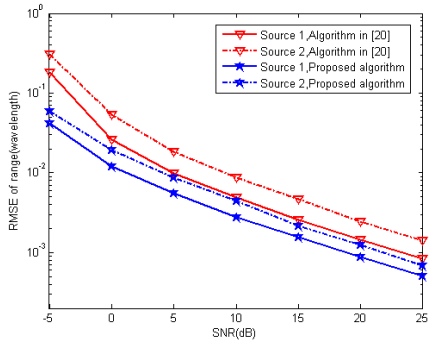

Figure 4. The RMSE of range estimates of both the algorithm in [20] and proposed algorithm versus SNR.

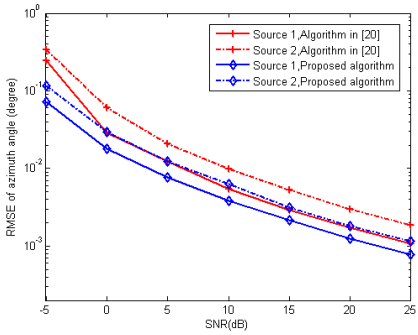

Figure 5. The RMSE of azimuth angle estimates of both the algorithm in [20] and proposed algorithm versus SNR.

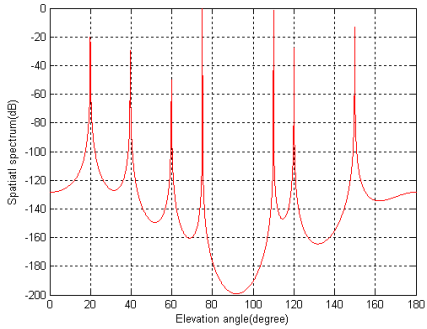

Figure 6. The spatial spectrum of elevation angle of the proposed algorithm.

RMSE difference of the elevation angle estimates of both the proposed algorithm and algorithm in [20] is larger than the RMSE difference of their range estimates, and the RMSE difference of their azimuth angle estimates is the smallest, which can be explained by the fact that in the proposed algorithm the range estimates are based on the elevation angle estimates and the azimuth angle estimates are based on both the elevation angle and range estimates; however, in the algorithm in [20], both the estimates of both the elevation and azimuth angles are obtained in the similar method, and thus the algorithm in [20] obtains approximate estimation accuracy of both the elevation and azimuth angles. Besides, in low SNR, the estimation performance of the proposed algorithm is more superior to that of the algorithm in [20], and thus the proposed algorithm is able to be used even in the environment of low SNR.

4.2. Capacity of Dealing with the Number of Signal Sources

In the second experiment, the capacity that the proposed algorithm simultaneously deals with the number of sources is examined. The seven NF sources are located at $\{\theta_1 = 20^\circ, r_1 = 11\lambda, \varphi_1 = 150^\circ\}$, $\{\theta_2 = 40^\circ, r_2 = 8\lambda, \varphi_2 = 105^\circ\}$, $\{\theta_3 = 60^\circ, r_3 = 9\lambda, \varphi_3 = 65^\circ\}$, $\{\theta_4 = 75^\circ, r_4 = 10\lambda, \varphi_4 = 45^\circ\}$, $\{\theta_5 = 110^\circ, r_5 = 15\lambda, \varphi_5 = 130^\circ\}$, $\{\theta_6 = 120^\circ, r_6 = 12\lambda, \varphi_6 = 80^\circ\}$ and $\{\theta_7 = 150^\circ, r_7 = 18\lambda, \varphi_7 = 30^\circ\}$, respectively. The snapshot number is set equal to 1000 and SNR is 5 dB. According to the analysis in Section 3.6, when each branch of the cross array is composed of 9 ($M = 4$) omnidirectional sensors, the

algorithm in [20] at most locates $M = 4$ sources, while the proposed algorithm can at most locate $2M - 1 = 7$ sources. From Figs. 6, 7 and Table 1, we observe that the proposed algorithm has the ability to accurately and simultaneously deal with seven sources, and thus these results are consistent with the theoretical analysis results in Section 3.

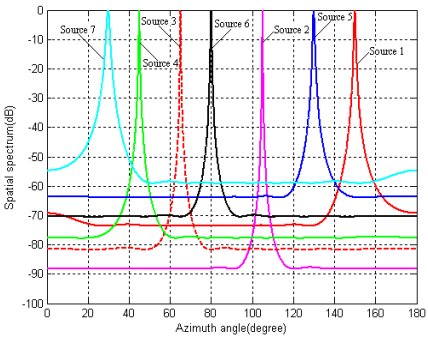

Figure 7. The spatial spectrum of azimuth angle of the proposed algorithm.

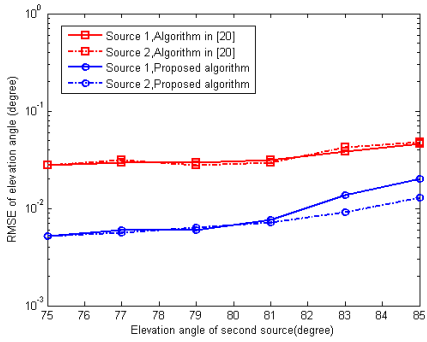

Figure 8. The RMSE of elevation angle estimates for two NF sources using the proposed algorithm and the algorithm in [20] when the elevation angle of the second source varies.

Table 1. The true value and estimated value of the range parameters of the proposed algorithm.

Source (Range)	**1**	**2**	**3**	**4**
True value	11λ	8λ	9λ	10λ
Estimated value	11.013λ	8.009λ	8.996λ	10.011λ
Source (Range)	**5**	**6**	**7**	
Ture value	15λ	12λ	18λ	
Estimated value	15.017λ	11.985λ	18.019λ	

4.3. Resolution [26, 27]

In the third experiment, we evaluate the resolution of the elevation angle, when the elevation angle of one NF source is close to that of another source. Two NF sources are located at $\{\theta_1 = 90°, r_1 = 6\lambda, \varphi_1 = 60°\}$ and $\{\theta_2 = 75° + \eta_1\theta, r_2 = 6\lambda, \varphi_2 = 60°\}$ respectively, with $\eta_1\theta$ varying in the range $[0°, 10°]$ by steps of $2°$. The SNR is fixed at 5 dB and snapshots number is set to 800. Fig. 8 shows that

when the angular gap of the elevation angle of the two NF sources becomes small gradually, the RMSEs of the elevation angle estimates of both the proposed algorithm and the algorithm in [20] increase, whereas the RMSEs of the proposed algorithm are always smaller than that of the algorithm in [20], which indicates that the proposed algorithm has better elevation angle resolution and estimation accuracy than the algorithm in [20]; this can be explained that the number of virtual sensors in the proposed algorithm is larger than that in the algorithm in [20]; in other words, the proposed algorithm has larger array aperture. Also, it can be seen from Figs. 9 and 10 that the proposed algorithm still has better estimation performance in range and azimuth angle estimates than the algorithm in [20]. Moreover, the range estimation of the algorithm in [20] is more sensitive to the angular gap of the elevation angle than the proposed algorithm; however, the elevation and azimuth angle estimation of the algorithm in [20] is more insensitive to the angular gap of the elevation angle than the proposed algorithm, which is consistent with the results in [20]. The results in this experiment validate the theoretical analysis result that the proposed algorithm has larger array aperture and is able to locate more sources than the algorithm in [20].

In the fourth experiment, considering the range of one NF source is close to that of another NF source, the resolution of the range is investigated. Two NF sources are located at $\{\theta_1 = 30°, r_1 = 6\lambda, \varphi_1 = 40°\}$ and $\{\theta_2 = 60°, r_2 = 6\lambda + \eta_2\lambda, \varphi_2 = 70°\}$ respectively, with

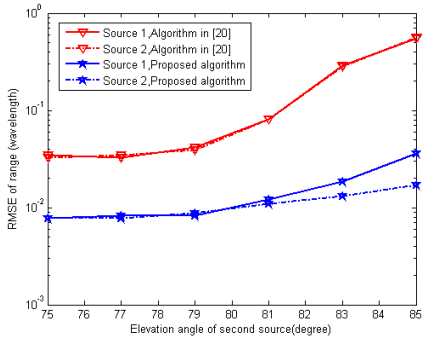

Figure 9. The RMSE of range estimates for two NF sources using the proposed algorithm and the algorithm in [20] when the elevation angle of the second source varies.

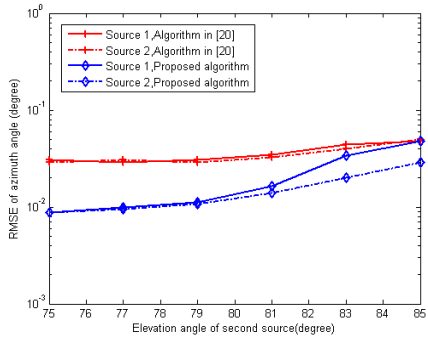

Figure 10. The RMSE of azimuth angle estimates for two NF sources using the proposed algorithm and the algorithm in [20] when the elevation angle of the second source varies.

$\eta_2\lambda$ varying in the range $[-0.5\lambda, 0.5\lambda]$ by steps of 0.1λ. SNR is fixed at 5 dB and snapshots number is set to 800. We can observe from Figs. 11, 12 and 13 that the proposed algorithm generally outperforms the algorithm in [20] with the range of the second source increasing, because of the large array aperture of the proposed algorithm. Moreover, from Fig. 11, it can be seen that the elevation angle estimates in both algorithms are insensitive to the change of range of second source. This is because that when estimating the elevation angle parameters, both the algorithm in [20] and proposed algorithm are separated from the range parameters. In Fig. 12, we can see that owing to the unchangeable range of first source, the RMSEs of range estimates of first source remain about the same; while due to the continuous change of range of second source from small to large, the RMSEs of range estimates of second source continually change from small to large. These phenomena agree with the analysis results in [14]. In Fig. 13, the RMSEs of the azimuth angle estimates in the algorithm in [20] is insensitive to the change of range of the second source, because the process of estimating the azimuth angle is independent with that of estimating the range; however, in the proposed algorithm since the azimuth angle are obtained based on the range estimates, the changing trends of the RMSEs of the azimuth angle estimates is similar to that of RMSEs of the range estimates.

In the fifth experiment, we test the resolution of the azimuth angle, when the azimuth angle of one NF source is close to that of another NF source. Two NF sources are located at $\{\theta_1 = 70°, r_1 = 6\lambda, \varphi_1 = 145°\}$ and $\{\theta_2 = 120°, r_2 = 5\lambda, \varphi_2 = 135° + \eta_3\varphi\}$, with $\eta_3\varphi$ varying in the

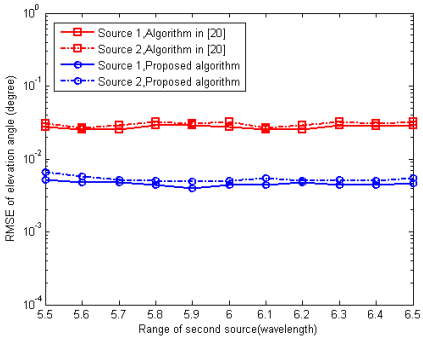

Figure 11. The RMSE of elevation angle estimates for two NF sources using the proposed algorithm and the algorithm in [20] when the range of the second source varies.

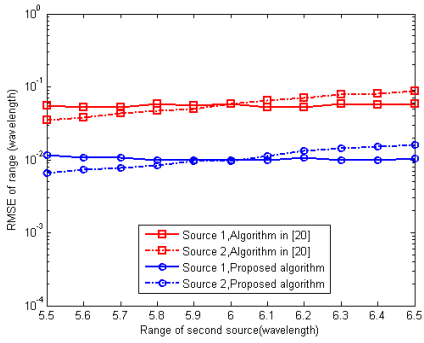

Figure 12. The RMSE of range estimates for two NF sources using the proposed algorithm and the algorithm in [20] when the range of the second source varies.

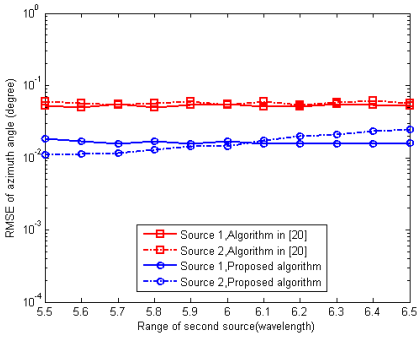

Figure 13. The RMSE of azimuth angle estimates for two NF sources using the proposed algorithm and the algorithm in [20] when the range of the second source varies.

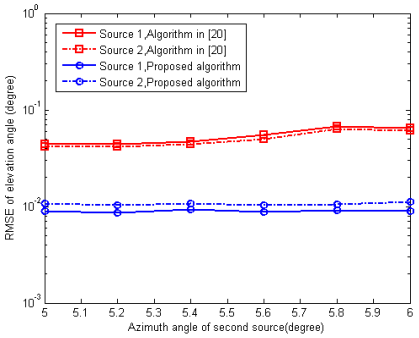

Figure 14. The RMSE of elevation angle estimates for two NF sources using the proposed algorithm and the algorithm in [20] when the azimuth angle of the second source varies.

range [0°, 10°] by steps of 2°. SNR is 5 dB and snapshots number is 500. Figs. 14 and 15 tell us that when the azimuth of the second source changes, the RMSEs of the elevation angle and range estimates of the proposed algorithm are almost unchanged; this is because that their estimates are independent with the azimuth angle parameter according to (45) and (51). However, as the azimuth angle of the second source is close to that of the first source, the estimation performance of the azimuth angle degrades slowly. It can be seen from Figs. 14, 15 and 16 that in the proposed algorithm the RMSEs of azimuth angle estimates are higher than that of range estimates and the RMSEs of elevation angle estimates are the lowest; because in the proposed algorithm, the range estimates are obtained based on the elevation angle estimates, and the azimuth angle estimates are estimated with both the elevation angle and range estimates. Moreover, in the whole change process of the azimuth angel of the second source, the proposed algorithm has better estimation accuracy of the elevation angle, range and azimuth angle than the algorithm in [20] because of the large array aperture of the proposed algorithm.

In the last experiment, the computational complexity and execution time of the proposed algorithm are compared with the 3D search algorithm in [21, 22]. The number of sensors and signal source are set to 18 and 2, respectively. Define $\Delta\theta = 0.1°$, $\Delta r = 0.1\lambda$ and $\Delta\varphi = 0.1°$, where $\Delta\theta$, Δr and $\Delta\varphi$ are the search step of elevation angle $\theta \in [0, \pi]$, range $r \in (0.62(D^3/\lambda)^{1/2}, 2D^2/\lambda)$ and azimuth

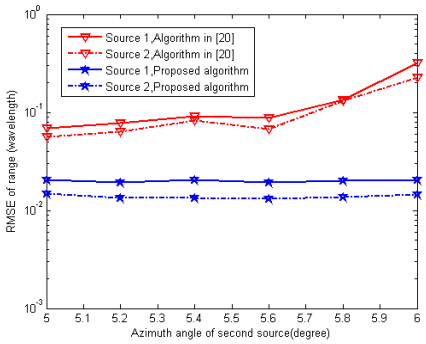

Figure 15. The RMSE of range estimates for two NF sources using the proposed algorithm and the algorithm in [20] when the azimuth angle of the second source varies.

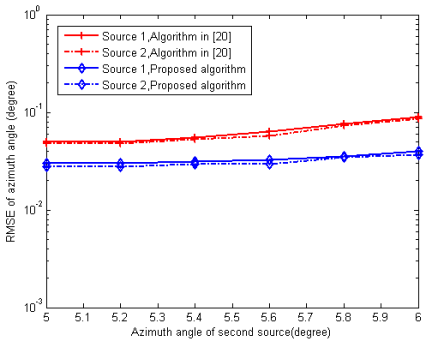

Figure 16. The RMSE of azimuth angle estimates for two NF sources using the proposed algorithm and the algorithm in [20] when the azimuth angle of the second source varies.

angle $\varphi \in (0, 2\pi]$, respectively. In order to obtain the 3D estimation parameters $\{\hat{\theta}_k, \hat{r}_k, \hat{\varphi}_k\}$ of all sources, the proposed algorithm spends 1.236 seconds execution time, while the 3D search algorithm in [21, 22] spends 3.627 seconds execution time. This is because that the proposed algorithm requires only 1D search, while the 3D search algorithm in [21, 22] needs to execute 3D search.

5. CONCLUSION

In this paper, based on the AE we present a 3D NF source localization algorithm to jointly estimate the elevation angle, range and azimuth angle parameters. Compared with the conventional 3D NF sources localization algorithm, the proposed algorithm has the following merits:

i): being different from the conventional algorithms, the proposed algorithm overcome the quarter-wavelength sensor spacing constraint so as to gain larger array aperture, and thus obtains better estimation performance than the conventional algorithms

ii): being different from the conventional algorithms, the number of sources which the proposed algorithm at most locates can exceeds the number of the sensors in each branch of the cross array.

iii): the proposed algorithm does not require extra parameters match procedure.

iv): the proposed algorithm replaces the 3D search required in conventional 3D MUSIC algorithms with 1D search, and HOS required in conventional 3D NF source localization algorithms with SOS, and thus reduces the computational burden.

v): based on the large array aperture and superior parameters estimation performance, the proposed algorithm gains higher parameters estimation resolution.

ACKNOWLEDGMENT

This work was supported in part by the National Natural Science Foundation of China under Grant 51275349 and 50375110, in part by the China New Century Excellent Talents in funding this project Grant NECT, in part by the China Tianjin Science and Technology to support key projects Grant 11ZCKFGX03600 and in part by the China Tianjin Science and Technology Sea Project Grant KX2010-0006.

REFERENCES

1. Krim, H. and M. Viberg, "Two decades of array signal processing research: The parametric approach," *IEEE Signal Process. Mag.*, Vol. 13, No. 4, 67–94, 1996.
2. Schmidt, R. O., "Multiple emitter location and signal parameters estimation," *IEEE Trans. on Antennas and Propagat.*, Vol. 34, No. 3, 267–280, Mar. 1986.
3. Roy, R. and T. Kailath, "ESPRIT — Estimation of signal parameters via rotational invariance technique," *IEEE Trans. on Acoust., Speech, Signal Processing*, Vol. 37, No. 7, 984–995, Jul. 1989.
4. Lizzi, L., F. Viani, M. Benedetti, P. Rocca, and A. Massa, "The M-DSO-ESPRIT method for maximum likelihood DOA estimation," *Progress In Electromagnetics Research*, Vol. 80, 477–497, 2008.
5. Changuel, H., F. Harabi, and A. Gharsallah, "2-L-shape two-dimensional arrival angle estimation with a classical subspace algorithm," *Progress In Electromagnetics Research*, Vol. 66, 301–315, 2006.
6. Yang, P., F. Yang, and Z.-P. Nie, "DOA estimation with sub-array divided technique and interporlated ESPRIT algorithm on a cylindrical conformal array antenna," *Progress In Electromagnetics Research*, Vol. 103, 201–216, 2010.
7. Piya, P. and P. P. Vaidyanathan, "Nested arrays: A novel approach to array processing with enhanced degrees of freedom,"

IEEE Transactions on Signal Processing, Vol. 58, No. 8, 4167–4181, 2010.

8. Cheng, S.-C. and K.-C. Lee, "Reducing the array size for DOA estimation by an antenna mode switch technique," *Progress In Electromagnetics Research*, Vol. 131, 117–134, 2012.
9. Liang, J. L. and D. Liu, "Joint elevation and azimuth direction finding using L-shaped array," *IEEE Trans. on Antennas and Propagat.*, Vol. 58, No. 6, 2136–2141, 2010.
10. Liang, J. and D. Liu, "Two L-shaped array-based 2-D DOAs estimation in the presence of mutual coupling," *Progress In Electromagnetics Research*, Vol. 112, 273–298, 2011.
11. Li, Y. and H. Ling, "Improved current decomposition in helical antennas using the ESPRIT algorithm," *Progress In Electromagnetics Research*, Vol. 106, 279–293, 2010.
12. Swindlehurst, A. L. and T. Kailath, "Near-field source parameter estimation using a spatial Wigner distribution approach," *Proc. SPIE Conf. 975*, 86–92, San Diego, CA, 1988.
13. Huang, Y. D. and M. Barkat, "Near-field multiple sources localization by passive sensor array," *IEEE Trans. on Antennas and Modeling Propag.*, Vol. 39, No. 7, 968–975, 1991.
14. Yuen, N. and B. Friedlander, "Performance analysis of higher order ESPRIT for localization of near-field sources," *IEEE Transactions on Signal Processing*, Vol. 46, No. 3, 709–719, 1998.
15. Challa, R. N. and S. Shamsunder, "High-order subspace based algorithms for passive localization of near-field sources," *Proc. 29th Asilomar Conf. Signals, Syst.*, Vol. 2, 777–781, Comput., Pacific Grove, CA, 1995.
16. He, J., M. N. S. Swamy, and M. O. Ahmad, "Efficient application of MUSIC algorithm under the coexistence of far-field and near-field sources," *IEEE Transactions on Signal Processing*, Vol. 60, No. 4, 2066–2070, 2012.
17. Grosicki, E., K. Abed-Meraim, and Y. Hua, "A weighted linear prediction method for near-field source localization," *IEEE Transactions on Signal Processing*, Vol. 53, No. 10, 3651–3660, 2005.
18. Challa, R. N. and S. Shamsunder, "3-D spherical localization of multiple non-Gaussian sources using cumulants," *8th Sag. Proc. Workshop on SSAP*, 101–104, Corfu, Greece, 1996.
19. Challa, R. N. and S. Shamsunder, "Passive near-field localization of multiple non-Gaussian sources in 3-D using cumulants," *Signal Process.*, Vol. 65, 39–53, 1998.

20. Abed-Meraim, K. and Y. Hua, "3-D near field source localization using second order statistics," *Conference Record of the Thirty-First Asilomar Conference on Signals, Systems & Computers*, Vol. 2, 1307–1311, 1997.
21. Hung, H.-S., S.-H. Chang, and C.-H. Wu, "3-D MUSIC with polynomial rooting for near-field source localization," *Conference Proceedings, 1996 IEEE International Conference on Acoustics, Speech, and Signal Processing, ICASSP-96*, Vol. 6, 3065–3069, Atlanta, Georgia, May 1996.
22. Hung, H.-S., S.-H. Chang, and C.-H. Wu, "Near-field source localization using MUSIC with polynomial rooting," *Journal of Marine Science and Technology*, Vol. 6, No. 1, 1–7, 1998.
23. Lee, C. M., K. S. Yoon, J. H. Lee, and K. K. Lee, "Efficient algorithm for localizing 3-D narrowband multiple sources," *IEEE Proc., Radar Sonar Navig.*, Vol. 148, No. 1, 23–26, 2001.
24. Lee, J. H., D. H. Park, G. T. Park, and K. K. Lee, "Algebraic path-following algorithm for localizing 3-D near-field sources in uniform circular array," *Electronics Letters*, Vol. 39, No. 7, 1283–1285, 2003.
25. Kabaoglu, N., H. A. Crpan, E. Cekli, and S. Paker, "Maximum likelihood 3-D near-field source localization using the EM algorithm," *Proceedings of the Eighth IEEE International Symposium on Computers and Communication*, Vol. 1, 492–497, Jun.-Jul. 3, 2003.
26. Dogan, M. C. and J. M. Mendel, "Applications of cumulants to array processing — Part I: aperture extension and array calibration," *IEEE Transactions on Signal Processing*, Vol. 43, 1200–1216, May 1995.
27. McCloud, M. L. and L. L. Scharf, "A new subspace identification algorithm for high-resolution DOA estimation," *IEEE Trans. on Antennas and Propagat.*, Vol. 50, 1382–1390, Oct. 1995.
28. Yang, K., Z. Q. Zhao, and Q. H. Liu, "Robust adaptive beamforming against array calibration errors," *Progress In Electromagnetics Research*, Vol. 140, 341–351, 2013.
29. Amar, J. G., "The Monte Carlo method in science and engineering," *Computing in Science & Engineering*, Vol. 8, No. 2, 9–19, Mar. 2006.
30. Metropolis, N. C., et al., "Equation of state calculations by fast computing machines," *J. Chemical Physics*, Vol. 21, 1087–1092, 1953.